Published in final edited form as:
Hear Res. 2011 December ; 282(1-2): 184–195. doi:10.1016/j.heares.2011.08.005.

Mature middle and inner ears express *Chd7* and exhibit distinctive pathologies in a mouse model of CHARGE syndrome

Elizabeth A. Hurd[a], **Meredith E. Adams**[c], **Wanda S. Layman**[b], **Donald L. Swiderski**[d], **Lisa A. Beyer**[d], **Karin E. Halsey**[d], **Jennifer M. Benson**[d], **Tzy-Wen Gong**[d], **David F. Dolan**[d], **Yehoash Raphael**[d], and **Donna M. Martin**[a,b]

[a]Department of Pediatrics, 3520A MSRB I, University of Michigan, Ann Arbor, MI 48109-5652, USA

[b]Department of Human Genetics, 3520A MSRB I, University of Michigan, Ann Arbor, MI 48109-5652, USA

[c] Department of Otolaryngology – Head & Neck Surgery, University of Michigan, 1904 Taubman Center, 1500 E. Medical Center Drive, Ann Arbor, MI 48109-5312 USA; meadams@umn.edu (M. Adams)

[d]Kresge Hearing Research Institute, Department of Otolaryngology, University of Michigan, Ann Arbor, MI 48109-5648, USA

Abstract

Heterozygous mutations in the gene encoding chromodomain-DNA-binding-protein 7 (CHD7) cause CHARGE syndrome, a multiple anomaly condition which includes vestibular dysfunction and hearing loss. Mice with heterozygous *Chd7* mutations exhibit semicircular canal dysgenesis and abnormal inner ear neurogenesis, and are an excellent model of CHARGE syndrome. Here we characterized *Chd7* expression in mature middle and inner ears, analyzed morphological features of mutant ears and tested whether *Chd7* mutant mice have altered responses to noise exposure and correlated those responses to inner and middle ear structure. We found that *Chd7* is highly expressed in mature inner and outer hair cells, spiral ganglion neurons, vestibular sensory epithelia and middle ear ossicles. There were no obvious defects in individual hair cell morphology by Prestin immunostaining or scanning electron microscopy, and cochlear innervation appeared normal in $Chd7^{Gt/+}$ mice. Hearing thresholds by auditory brainstem response (ABR) testing were elevated at 4 and 16 kHz in $Chd7^{Gt/+}$ mice, and there were reduced distortion product otoacoustic emissions (DPOAE). Exposure of $Chd7^{Gt/+}$ mice to broadband noise resulted in variable degrees of hair cell loss which inversely correlated with severity of stapedial defects. The degrees of hair cell loss and threshold shifts after noise exposure were more severe in wild type mice than in mutants. Together, these data indicate that $Chd7^{Gt/+}$ mice have combined conductive and sensorineural hearing loss, correlating with changes in both middle and inner ears.

Keywords

CHARGE syndrome; CHD7; inner ear; cochlea; noise exposure; middle ear

Corresponding author Donna Martin MD PhD 3520A MSRB I, 1500 W. Medical Center Drive, University of Michigan, Ann Arbor, MI 48109-5652 Tel: (734) 647-4859, Fax: (734) 763-9512, donnamm@med.umich.edu .
lizhurd@med.umich.edu (E. Hurd); layman@med.umich.edu (W. Layman); donnamm@umich.edu (D. Martin)
matuszew@umich.edu (J. Benson); lbeyer@umich.edu (L. Beyer); ddolan@umich.edu (D. Dolan); tzywen@umich.edu (T. Gong); khalsey@umich.edu (K.Halsey); dlswider@umich.edu (D. Swiderski); yoash@umich.edu (Y. Raphael)
ME Adams (current address): Department of Otolaryngology, 420 Delaware Street S.E., Mayo Clinic Code 396, Minneapolis, MN 55455;

1. Introduction

Haploinsufficiency for *CHD7*, the gene encoding the ATP dependent chromodomain protein 7, causes human CHARGE syndrome, a multiple congenital anomaly disorder characterized by ocular coloboma, heart defects, atresia of the choanae, retarded growth and development, genital hypoplasia, ear abnormalities, and brainstem/cranial nerve dysfunction (Vissers et al., 2004). Most *CHD7* mutations in CHARGE syndrome are loss of function alleles thought to render the CHD7 protein unstable or nonfunctional (Zentner et al., 2010). CHD7 is a nuclear localized protein that participates in large complexes which bind DNA and regulate access to chromatin and modulate gene transcription (Martin, 2010). The clinical features of CHARGE are highly variable and incompletely penetrant, with the most frequent defects occurring in the ear (Jongmans et al., 2006; Lalani et al., 2006). The most common clinical ear abnormalities among *CHD7*-mutation positive individuals are hearing loss (HL), temporal bone anomalies including semicircular canal hypoplasia, and auricular malformations (Zentner et al., 2010). Semicircular canal hypoplasia/dysplasia is a highly diagnostic feature in CHARGE syndrome that contributes to vestibular areflexia and impaired motor development (Abadie et al., 2000; Admiraal et al., 1997; Tellier et al., 1998; Wiener-Vacher et al., 1999).

The hearing abilities of CHARGE individuals are highly variable. As many as 80-85% of individuals with CHARGE have HL, but there is marked variability in the type of HL and the degree to which each individual is affected (Edwards et al., 2002). Among those with hearing impairment, losses vary from mild (> 20dB) to profound (> 90dB), with the majority (80%) having at least a moderate (> 40dB) HL in the better hearing ear (Dhooge et al., 1998; Edwards et al., 1995; Edwards et al., 2002; Morgan et al., 1993; Shah et al., 1998; Thelin et al., 1986). CHARGE-associated HL may be unilateral or bilateral, and conductive, sensorineural, or mixed (Edwards et al., 2002; Shah et al., 1998). While the sensorineural component remains stable over time, chronic or recurrent otitis media with effusion secondary to Eustachian tube dysfunction is associated with reports of fluctuating or progressive conductive HL (Edwards et al., 2002; Shah et al., 1998).

Mice with heterozygous *Chd7* loss of function mutations are an excellent model for CHARGE syndrome (Bosman et al., 2005; Hurd et al., 2007). Here, we studied $Chd7^{Gt/+}$ mice which are heterozygous for a gene trap-derived null allele ($Chd7^{Gt}$) that expresses β-galactosidase under the control of the *Chd7* promoter, as previously described (Hurd et al., 2007). $Chd7^{Gt/+}$ mice display severe inner ear defects characteristic of CHARGE syndrome, including variable and asymmetric hypoplasia of the lateral and posterior semicircular canals, and defects in vestibular sensory epithelial innervation (Adams et al., 2007; Hurd et al., 2010; Hurd et al., 2007). The auditory function of $Chd7^{Gt/+}$ mice has not yet been fully characterized, and it is not known whether *Chd7* mutant ears exhibit altered responses to environmental injury. We examined *Chd7* β-galactosidase reporter expression in the mouse cochlea and vestibular organs to determine precisely which mature cell types express *Chd7*, characterized the mature *Chd7* mutant inner ear sensory epithelium using light microscope histology, immunofluorescence and scanning electron microscopy, and examined *Chd7* mutant middle ear bones for morphological abnormalities. We used physiological measures (ABR and DPOAE) to determine whether auditory response to noise is affected by *Chd7* haploinsufficiency. Our results indicate mixed sensorineural and conductive HL in $Chd7^{Gt/+}$ mice, with evidence of protection from noise that is likely associated with structural abnormalities of the stapes. These results have implications for understanding the human hearing phenotypes in CHARGE patients.

2. Materials and Methods

2.1 Mice

Congenic *Chd7*$^{Gt/+}$ mice on a 129S1/Sv1mJ background were mated with F1 hybrid B6D$_2$F$_1$/J (Jackson laboratory, Bar Harbor, ME #100006) mice to generation N4-N5 to improve fertility and genotyped as previously described (Hurd et al., 2007). Mice were also genotyped for the age related HL *Cdh23*^{ahl} allele, as described (Noben-Trauth et al., 2003). Experiments were performed on male and female postnatal day 1 or adult (5-12 week) sex-matched, age-matched littermate *Chd7*$^{Gt/+}$ and *Chd7*$^{+/+}$ mice. All procedures were approved by the University Committee on Use and Care of Animals at the University of Michigan.

2.2 β–Galactosidase Histochemistry

Chd7$^{Gt/+}$ mice were anesthetized, perfusion fixed with 4% paraformaldehyde and temporal bones removed from the head. Ears were fixed locally by opening the oval and round windows, perforating the apical end of the cochlea, and gently perfusing 4% paraformaldehyde for 1 hour. Specimens were washed in X-gal wash buffer (sodium phosphate buffer pH 7.4 with 2 mM $MgCl_2$ and 0.02% NP-40 (Sigma, St Louis, MO)), and incubated for 72 hours in X-gal wash buffer containing 1mg X-gal (Invitrogen, Carlsbad, CA), 5 mM potassium ferro-cyanide (Fisher, Pittsburgh, PA), 5 mM potassium ferricyanide (Fisher), and 0.33% N-N-dimethylformamide (Sigma). Upon completion of fixation, middle ears were removed and photographed and cochleae were transferred to wash buffer, decalcified in 3% EDTA (Ethylenediaminetetraacetic acid) (pH7.3-7.4) for 24 hours and cryoprotected in 30% sucrose overnight at 4°C. Ears were flash frozen in O.C.T. embedding medium (Tissue Tek, Torrance, CA, USA) and cryosectioned at 12 μm. Sections were either stained with eosin or incubated with a 200-kDa anti-mouse Neurofilament antibody (1:200 Sigma, no. N0142) and processed for immunohistochemistry with DAB (3,3′-Diaminobenzidine, Sigma). Slides were mounted and images captured on a Leica DMRB microscope.

2.3 Wholemount immunofluorescence

Inner ears from adult *Chd7*$^{Gt/+}$ and wild type mice were isolated and fixed as described above. Cochleae were isolated and permeabilized with 0.3% Triton X-100 in PBS and blocked in either normal goat or normal donkey serum (1%) and bovine serum albumin (0.1%) for 30 minutes. Primary antibodies were incubated for 1 hr at room temperature: mouse anti-neurofilament (1:200, Sigma), rabbit anti-myosin VIIa (1:200, Proteus Biosciences, Ramona, CA no. 25-6790), and goat anti-Prestin (1:100, Santa Cruz, Santa Cruz, CA, no. sc-22694). Cochleae were incubated with Alexa Fluor 488 and Alexa Fluor 595 conjugated secondary antibodies (Invitrogen) for 1 hr at room temperature before being washed, mounted and imaged on a Leica DMRB microscope.

2.4 Scanning Electron Microscopy (SEM)

For SEM analysis, 6-week-old *Chd7*$^{Gt/+}$ and sex-matched littermate wild type mice were anesthetized and perfusion fixed with 2% glutaraldehyde in 0.15M cacodylate buffer (pH 7.2-7.4). Temporal bones were removed, cochleae exposed, and samples fixed in a solution of 3% glutaraldehyde, 2% paraformaldehyde, 1% acrolein in 0.1M cacodylate buffer (pH 7.2-7.4). Tissues were processed using the OTOTO (Osmium –thiocarbohydrazide) method then dehydrated in increasing concentrations of ethanol and critical point dried with CO_2 in a SamDri 790 (Tousmis, Rockville, MD)(Osborne et al., 1991) before being examined on an Amray 1910 Field Emission Scanning Electron Microscope and photographed digitally using X-Stream software.

2.5 Light microscopy sections

Adult (6-8 week-old) ears were obtained and fixed as described above for SEM. Tissues were decalcified and embedded in EMBED-812 (Electron Microscopy Sciences, Hatfield, PA). Cochleae were sectioned in a mid-modiolar plane 1 μm and the sections stained with Toluidine Blue (Electron Microscopy Sciences) and analyzed on a Leica DMRB light microscope with a 100x objective lens.

2.6 Auditory Brainstem Response (ABR) testing and noise exposure

Adult *Chd7*$^{Gt/+}$ and wild type mice were anesthetized, and ABRs recorded in an electrically and acoustically shielded chamber (Acoustic Systems, Austin, TX USA) as previously described (Beyer et al., 2000; Karolyi et al., 2007). Briefly, needle electrodes were placed at vertex (active) and the test ear (reference) and contralateral (ground) ear pinnae. Tucker Davis Technologies (TDT) System III hardware and SigGen/BioSig software (TDT, Alachua, FL USA) were used to present the stimulus and to record responses. Tones were delivered through an EC1 driver (TDT, aluminum enclosure made in-house), with the speculum placed just inside the tragus. Stimuli were 15 ms tone bursts, with 1 ms rise/fall times, presented 10 per second. Stimulus intensities typically ranged from 0-80 dB SPL, higher if needed to obtain a response, up to the system limit of 110 dB SPL. Up to 1024 responses were averaged for each stimulus level. Responses were collected for stimulus levels in 10 dB steps at higher stimulus levels, with additional 5 dB steps near threshold. Thresholds were interpolated between the lowest stimulus level where a response was observed, and 5 dB lower, where no response was observed. Thresholds were measured for 4, 16, and 32 kHz stimuli.

2.7 Distortion Product Otoacoustic Emissions (DPOAE) testing

Mice were anaesthetized with ketamine and xylazine to ensure immobilization and relaxation. DPOAE tests were measured at 5 weeks of age in left ears at 8, 16 and 24 kHz as previously described (Karolyi et al., 2007), on the same cohort of mice that underwent ABR testing. Briefly, primary tones, *f*1 and *f*2, were set at a ratio of *f*2/*f*1= 1.2. Intensity of *f*1 was varied in 5-10 dB SPL steps, while *f*2 intensity was held 10 dB SPL quieter than *f*1. Tones were presented via two EC1 drivers (Beyerdynamic Inc., Farmingdale, NY; Aluminum-shielded enclosure made in-house) connected through an Etymotic microphone (Etymotic Research Inc., Elk Grove Village, IL, ER 10B+). TDT System II hardware and SigGen/BioSig software were used to present the stimuli and to record responses.

2.8 Noise Exposure

After ABR and DPOAE testing, wild type (N=12) and *Chd7*$^{Gt/+}$ (N=17) were exposed to 123 dB broadband noise for 4.5 hrs. After a 2 week recovery period, mice underwent ABR testing and were euthanized. Cochleae were dissected, fixed and immunostained as described above, then dissected as wholemounts for analysis. For a subset of mice (5 wild type and 7 *Chd7*$^{Gt/+}$), left middle ear ossicles were dissected by a blinded observer and photographed on a Leica microscope.

2.9 Statistical analysis

To test for differences in hearing between *Chd7*$^{Gt/+}$ mice and wild type littermates, ABR thresholds were evaluated by MANOVA, with significance ($p < 0.05$) determined by the F value calculated from Wilks' $\wedge$ and the corresponding degrees of freedom. Subsequently, *ad hoc* univariate Student's *t*-tests were performed on the data from each ABR test frequency to determine which ones contributed to the overall difference in hearing, with significance determined by sequential Bonferroni criterion to keep the table-wide error rate below 0.05. Correlations between middle ear bony abnormality and genotype were analyzed by two-by-

two contingency tables and significance ($p < 0.05$) determined from Chi-square distribution with one degree of freedom. After noise exposure, all but 2 mice (5 of 7 *Chd7*$^{Gt/+}$ and all 5 wild type mice) had undetectable ABR responses at or below the system limit of 110 dB SPL, at least one frequency (4, 16 and 32 kHz). Consequently, hearing abilities were scored as being above or below a given threshold; thus, analysis of variance could not be used, so two-by-two contingency tables were used to test for associations between hearing ability and genotype or middle ear bony abnormality.

3. Results

3.1 *Chd7* is expressed in discrete regions in the mature mouse inner ear

Previous studies identified *Chd7* expression in developing inner ear tissues in both humans and mice (Bosman et al., 2005; Hurd et al., 2010; Hurd et al., 2007; Sanlaville et al., 2006), but sites of CHD7 expression in mature tissues were not characterized. Here, we analyzed β-galactosidase staining in the mature *Chd7*$^{Gt/+}$ mouse inner ear. X-gal stained frozen sections of adult *Chd7*$^{Gt/+}$ mice showed β-galactosidase label in several cochlear tissues and cell types including the stria vascularis, Reissner's membrane, Boettcher's cells, inner hair cells (IHC), outer hair cells (OHC), spiral ligament, spiral limbus, inner and outer pillar cells, and spiral ganglion (SG) neurons (Fig. 1A-D). β-galactosidase activity in the cochlea was similar in intensity and distribution throughout the cochlea, from base to apex. Sections through the vestibular epithelium also showed β-galactosidase label in the sensory epithelium of the lateral canal crista and utricle of adult *Chd7*$^{Gt/+}$ mice (Fig. 1E-H). Since *Chd7* has been implicated in inner ear neurogenesis and olfactory sensory neuron formation (Hurd et al., 2010; Layman et al., 2011; Layman et al., 2009), we processed X-gal stained sections for immunohistochemistry with anti-neurofilament (Fig. 1B,D,F,H) to assess expression of *Chd7* within mature inner ear neurons. β-galactosidase activity was present in the cytoplasm of most neurofilament-positive cells within the spiral ganglion (Fig. 1D arrow) and vestibular epithelium (Fig. 1F, H). However, neurofilament-positive, *Chd7*-negative cells were also observed within the spiral ganglion (Fig. 1D arrowhead). These data show that *Chd7* is highly expressed within the mature cochlea and vestibular sensory epithelium, suggesting an ongoing role for *Chd7* in the adult inner ear.

3.2 *Chd7*$^{Gt/+}$ mice have mild low to mid-frequency hearing loss

Previous studies have demonstrated that *Chd7* mutant mice have mild HL, with elevated compound action potentials (Hawker et al., 2005; Lenz et al., 2010). Here, we measured auditory brainstem evoked response (ABR) as an indicator of hearing thresholds in sex-matched five-week old littermate *Chd7*$^{Gt/+}$ (N=17) and wild type (N=13) mice (Fig. 2). One *Chd7*$^{Gt/+}$ mouse had no response at 32 kHz at the system limit of 110 dB SPL. Threshold for this mouse was therefore treated as just above the system limits (which may underestimate the true mean and variance); however, excluding this mouse would underestimate the true mean and variance even more. MANOVA examination of all three tested frequencies showed significant differences in thresholds between *Chd7*$^{Gt/+}$ mice and wild type littermates ($F = 12.45$, df = 3 & 26, $p < 0.0001$). Univariate analysis showed that *Chd7*$^{Gt/+}$ mice had significantly higher mean ABR thresholds than wild type mice at 4 kHz (79 vs. 41 dB SPL, $p < 0.0001$) and 16 kHz (38 vs. 22 dB, $p < 0.009$), but not at 32 kHz (58 vs. 65 dB, $p > 0.4$) (Fig. 2). The majority of mice (N=10/13 wild type; N=12/17 *Chd7*$^{Gt/+}$) were homozygous for the *Cdh23*^{ahl} sensitive gene, which increases susceptibility to high-frequency HL at 8 weeks of age and to temporary threshold shifts due to noise exposure (Harding et al., 2005; Noben-Trauth et al., 2003).

3.3 Cochlear morphology and ultrastructure are normal in *Chd7$^{Gt/+}$* mutant mice

We next examined whether mild HL in *Chd7$^{Gt/+}$* mice was associated with changes in cochlear ultrastructure. Standard histology showed normal anatomy of the organ of Corti in both wild type and *Chd7$^{Gt/+}$* mice (Fig. 3A, B). Using scanning electron microscopy (SEM), we found a normal appearing pattern of stereocilia at the apical surface of the IHCs and OHCs in wild type mice and *Chd7$^{Gt/+}$* (Fig. 3C, D). Three rows of OHCs were observed in most cochlear regions, and both wild type and *Chd7$^{Gt/+}$* mice had short stretches (5-6 cells) of four rows of OHCs irregularly spaced predominantly in the apex, but these areas were more abundant in *Chd7$^{Gt/+}$*, consistent with our ABR data (Fig. 2) and with previous reports showing that intermittent supernumerary rows of hair cells may contribute to sensorineural HL in *Chd7* haploinsufficient mice (Pau et al., 2004).

We also examined expression of the membrane motor protein, Prestin, which is responsible for electromotility in OHCs (Dallos, 2008). No difference in Prestin expression was observed in the cochleae of *Chd7$^{Gt/+}$* mice compared to wild type littermates by wholemount immunofluorescence (Fig.3E, F). Cochleae of *Chd7$^{Gt/+}$* mice exhibited a fourth row of OHCs in some areas. The Prestin in the fourth row appeared similar in organization and label-intensity to that seen in the other rows of OHCs. Wholemounts of cochleae stained for neurofilament and myosin VIIa also showed normal appearing innervation of cochlear hair cells in *Chd7$^{Gt/+}$* and control mice (Fig 4). Together with the ABR results, these data suggest that the impairment of low-mid frequency auditory signals is not secondary to abnormalities in hair cell formation.

3.4 *Chd7$^{Gt/+}$* mice have flattened DPOAEs

Middle-ear conductive and inner-ear sensorineural HL (SNHL) can be distinguished readily in CHARGE individuals with behavioral audiometry by detection of an air-bone gap between air-conduction and bone-conduction thresholds (Edwards et al., 2002). Because CHARGE-associated HL may be conductive, sensorineural, or mixed, we performed DPOAE on a cohort of sex matched, five week old *Chd7$^{Gt/+}$* and wild type mice used for ABR analysis to assess the mechanical contribution to the elevated ABR thresholds observed. In the mid frequency range, flattened or absent DPOAEs were detected in the majority of *Chd7$^{Gt/+}$* mice at 8 kHz (N=7/8), 16 kHz (N=5/8) and 24 kHz (N=6/8) (Fig. 5). We observed an association between *Chd7$^{Gt/+}$* mice with distortion responses at 16 kHz and 24 kHz and milder HL by ABR analysis (N=3). The severity of the DPOAE deficiency and relatively mild elevation in ABR thresholds at low frequencies in *Chd7$^{Gt/+}$* mice suggests that, in addition to the mild to moderate sensorineural HL, these mice also exhibit conductive HL.

3.5 Resistance to noise exposure in *Chd7$^{Gt/+}$* mice

Maintenance of *Chd7* expression within the adult cochlea provides evidence of a role for *Chd7* within the mature inner ear, yet *Chd7^{Gt+}* mice have no visible neuronal or sensory defects within the organ of Corti (Figs 1-3). We hypothesized that *Chd7* may play a role in protecting the ear from trauma. To investigate this hypothesis, we exposed *Chd7$^{Gt/+}$* and wild type mice to 123 dB broadband noise. During noise exposure, a large number of *Chd7$^{Gt/+}$* mice died (N=7/17), potentially from seizures, but death did not correlate with pre-exposure auditory thresholds. We examined dissected cochleae for the presence of hair cells and innervation using myosin VIIa and neurofilament co-staining. Unexposed wild type mice (N=2) had no IHC or OHC loss, and no loss of innervation or alteration in auditory threshold at the end of the testing period (Fig. 6A, E, I). Noise-exposed wild type mice had mild loss of IHC and severe loss of OHC. In addition, the longitudinal and radial nerve fibers in the organ of Corti appeared reduced or absent, consistent with elevated post-exposure auditory thresholds (Fig. 6B, F). There was a gradient of hair cell loss and

innervation loss from base to apex in wild type mice, with the basal portion of the cochlea being more severely affected. *Chd7*$^{Gt/+}$ mice that survived noise exposure could be separated into 2 classes, those that demonstrated protection (N=6/10) (Fig. 6C, G, K) and those that did not (N=4/10) (Fig. 6D, H, L). *Chd7*$^{Gt/+}$ mice that were resistant to noise exposure (N=6/10) had no IHC or OHC loss, normal distribution of nerve fibers throughout the cochlea, and resembled unexposed wild type mice. Although auditory thresholds from noise-resistant *Chd7*$^{Gt/+}$ mice were elevated pre-exposure, the thresholds remained unchanged post-exposure, consistent with preservation of cochlear structure. *Chd7*$^{Gt/+}$ mice that were sensitive to noise (N=4/10) had mild loss of IHC, severe loss of OHC, and reduced or absent innervation similar to results seen in noise-exposed wild type mice.

3.6 Stapedial defects in *Chd7*$^{Gt/+}$ contribute to elevated auditory threshold and evidence of protection from noise exposure

Middle ear defects are associated with elevated ABR thresholds and abnormal DPOAE, and can contribute to protection from environmental injury (Gehr et al., 2004; Qin et al., 2010). We therefore analyzed middle ears isolated from a subset of wild type (N=5) and *Chd7*$^{Gt/+}$ (N=7) mice exposed to noise (described above). There was no obvious sign of infection (otitis media), debris in the ear cavity or abnormality in the tympanic membrane in any of the mice that we examined (N=12); however, oval and round windows of *Chd7*$^{Gt/+}$ mice were generally smaller than wild type mice (data not shown). Detailed examination of the ossicles showed no difference in the mallei between *Chd7*$^{Gt/+}$and wild type mice (Fig. 7A vs. B). In the incus, we observed a number of variations in wild type mice (N=3/5) including increased flexibility of the pedicle, variation in the angle between the long arm and the body of the incus, and abnormal shape of the malleal articulation within the head of the incus (Fig. 7C, E). These variant forms of the incus were also observed in *Chd7*$^{Gt/+}$ mice (N=7/7) (Fig. 7D, F), and were not significantly correlated with *Chd7* genotype ($p > 0.6$).

In contrast to the incus and malleus, careful examination of the stapes revealed defects in several *Chd7*$^{Gt/+}$ mice (N=5/7; vs. wild type N=0/5; $p < 0.013$) including flattened stapedial footplate, fusion of the stapedial footplate to the otic capsule, fusion of the stapedial arch to the dorsal wall of the middle ear cavity, and deflection and narrowing of the stapedial artery (Fig. 8A, B). Prior to noise exposure, ABR thresholds were generally lower in wild type mice than in *Chd7*$^{Gt/+}$ mice. At 4 kHz, all wild type mice (N=5) had thresholds less than 40 dB; the only *Chd7*$^{Gt/+}$ mouse (N=1/7) with a threshold less than 40 dB at 4 kHz had a free stapes. Similar results were observed at 16 kHz: all wild type mice had ABR thresholds less than 20 dB, whereas the only *Chd7*$^{Gt/+}$ mouse with a threshold less than 20 dB had a free stapes (and was not the same mouse that had a lower threshold at 4 kHz). At 32 kHz, most mice (N=3/5 wild type, N=4/7 *Chd7*$^{Gt/+}$) had ABR thresholds above 70 dB. These results indicate anassociation between HL prior to noise exposure and stapes fixation at 4 kHz and 16 kHz ($p<0.004$ and $p<0.006$, respectively), but not at 32 kHz ($p>0.9$).

To assess whether the effect of noise on ABR thresholds was moderated by stapedial fusion, we grouped the *Chd7*$^{Gt/+}$ mice with free stapes (N=2) together with the wild type mice (N=5), all with free stapes. ABR thresholds after noise were then compared between mice with free stapes (N=7) and mice with fixed stapes (all *Chd7*$^{Gt/+}$, N=5), regardless of genotype. After noise exposure, all 7 animals with free stapes had ABR thresholds above 110 dB at 4 kHz and above 80 dB at 16 kHz, representing threshold shifts > 55 dB for each animal at each frequency. Only one animal (*Chd7*$^{Gt/+}$) with a fixed stapes had an ABR threshold above 110 dB, and none had a threshold shift > 45 dB, at either 4 kHz or 16 kHz. At 32 kHz, 10 of the 12 mice had threshold shifts > 30 dB after noise exposure, including all 5 *Chd7*$^{Gt/+}$ mice with fixed stapes; the two exceptions were among the 4 wild type mice with thresholds ≥ 80 dB prior to noise exposure; thus, their low threshold shifts are likely due to extensive prior damage, not protection from noise exposure. At the lower frequencies

(4 and 16 kHz), protection against noise-induced HL in *Chd7*$^{Gt/+}$mice was strongly associated with stapedial fusion or partial ankylosis, (p<0.0006). These data suggest that the stapedial abnormalities in *Chd7*$^{Gt/+}$ mice confer protection of the inner ear against noise-induce injury.

3.7 *Chd7* is highly expressed in the middle ear

Middle ear development continues during the early postnatal period (as late as postnatal day 10), during which time the cartilage of the middle ear becomes ossified (Park, 1992). X-gal stained middle ears from postnatal day 1 *Chd7*$^{Gt/+}$ mice showed β-galactosidase activity in the developing malleus, incus, stapes, tympanic membrane, manubrium of the malleus and Meckel's cartilage (Fig. 9). A gradient of β-galactosidase activity was observed in Meckel's cartilage, from the connection with the malleus toward the dentary/mandible, and in the malleus from the posterior to the equally thick anterior end (Fig. 9A, C). There was no β-galactosidase staining between the malleus and incus, in the lenticular process of the incus or the capitulum of the stapes (Fig. 9B, E). In addition, there was no staining adjacent to the ventral portion of the stapedial footplate, where an incomplete oval window was formed. Dense β-galactosidase activity was observed in the stapedial footplate of *Chd7*$^{Gt/+}$ mice and also within the abnormal fused tissue between the dorsal stapes and cochlea wall, which is the most commonly fused area in the adult *Chd7*$^{Gt/+}$ mice (Fig. 9D, E). These data provide evidence that stapedial defects are visible in *Chd7*$^{Gt/+}$ mice as early as postnatal day 1. Expanded expression of *Chd7* during middle ear development correlates with fixation of the stapes to the cochlear wall and defects of the oval window observed in adult *Chd7*$^{Gt/+}$ mice.

4. Discussion

4.1 Summary

Here we demonstrate, using a *Chd7* null reporter allele, that *Chd7* is expressed in the mature organ of Corti, spiral ganglion, vestibular neurons and vestibular epithelium of the inner ear. *Chd7*$^{Gt/+}$ mice have minimal defects in cochlear morphology, yet display mild low- to mid-frequency HL and flattened DPOAEs. *Chd7* is also expressed in middle ear ossicles, and *Chd7*$^{Gt/+}$ mice have variably penetrant middle ear abnormalities which appear to correlate with extent of protection from noise exposure. The findings of combined conductive-sensorineural HL and resistance to overstimulation injury in *Chd7*$^{Gt/+}$ mice may have implications for the audiological management and treatment of CHARGE patients.

4.2 Middle ear abnormalities in *Chd7*$^{Gt/+}$ mice may provide protection from noise exposure

Several different spontaneous *Chd7* mutant mouse strains have been described, each of which is a loss of function allele (Bosman et al., 2005; Lenz et al., 2010). Like these spontaneous mutants, *Chd7*$^{Gt/+}$ mice are also heterozygous for a null allele, and have the added advantage of expressing β-galactosidase under the control of the *Chd7* promoter (Hurd et al., 2007). Because the majority of *CHD7* mutations in humans are also loss of function alleles, derived from nonsense mutations or *CHD7* gene deletions, *Chd7* heterozygous mutant mice are an especially good model for human CHARGE syndrome (Zentner et al., 2010). We observed mild elevations in auditory thresholds and variable ossicular abnormalities in *Chd7*$^{Gt/+}$ mice, similar to those observed in other *Chd7* mutant mice (Hawker et al., 2005; Kiernan et al., 2002; Lenz et al., 2010). Some *Chd7* mutant mice (*Flo*, *Whi*, *Crsl*) have a positive Preyer reflex with round window hypoplasia and variable malleal, incudal and stapedial defects (Hawker et al., 2005; Pau et al., 2004), suggesting variable effects of *Chd7* deficiency on hearing and middle ear formation. However, until now, stapedial abnormalities were not directly correlated with HL and protection from environmental injury. Unfortunately, *Chd7*$^{Gt/Gt}$ embryos do not survive past embryonic day10.5, precluding later analysis of homozygous *Chd7* mutant middle ears (Hurd et al.,

2007). Conditional loss of *Chd7* specifically within the middle ear has not yet been described, but the high penetrance of middle ear defects in heterozygous *Chd7* mutant mice and the rudimentary ear seen in early otocyst-specific conditional *Chd7* mutants (Hurd et al., 2010) suggests that complete loss of *Chd7* in the middle ear will result in severe abnormalities.

Chd7 function is also important for middle ear development in humans. A variety of middle ear abnormalities have been described in CHARGE individuals, including malleus fixation, absent malleus manubrium, hypoplasia/malunion of the incus, absent stapedial muscle, and atresia/absence of the stapes, oval window and round window (Haginomori et al., 2002; Lanson et al., 2007; Lemmerling et al., 1998; Morimoto et al., 2006; Shah et al., 1998). Temporal bone defects are a highly specific clinical criterion for diagnosing CHARGE syndrome (Amiel et al., 2001). Another prevalent feature in CHARGE patients is chronic otitis media with effusion (OME), which contributes to hearing impairment and may require surgical intervention (Shah et al., 1998). In humans, middle-ear conductive and inner-ear SNHL can be distinguished readily in CHARGE individuals with behavioral audiometry by detection of an air-bone gap between air-conduction and bone-conduction thresholds. However, it is more challenging to confirm conductive HL in mice, as there is no standardized method of murine bone conduction stimulation (Qin et al., 2010). The similarities in middle ear abnormalities between $Chd7^{Gt/+}$ mice and CHARGE individuals suggest common evolutionarily conserved mechanisms for *Chd7* function in middle ear development and maintenance.

Middle ear abnormalities are an important factor when considering surgical interventions for conductive and sensorineural HL. The likelihood of successfully repairing an ossicular chain defect is partly dependent on the presence or absence of a mobile, intact stapes. Traditional amplification or bone-anchored hearing aid (BAHA) placement may be more appropriate if a stapes defect is anticipated. For severe to profound SNHL in CHARGE patients, cochlear implant (CI) surgery has proven safe and effective in experienced hands, and the success of the implant is not dependent on the severity of ear abnormalities (Lanson et al., 2007). Nonetheless, there are considerable technical challenges during CI surgery in CHARGE patients secondary to the absence of normal surgical landmarks and variations in round window and cochlear morphology. Translation of data presented here to humans with CHARGE may assist surgeons when preparing and performing corrective surgery.

4.3 Etiology of sensorineural hearing loss in $Chd7^{Gt/+}$ mice

The mild elevation in auditory thresholds in $Chd7^{Gt/+}$ mice and the severity of DPOAE changes are consistent with combined sensorineural and conductive HL. The reduction in the measurable DPOAEs is likely augmented by the conductive component of the hearing impairment, which reduces both the input tones and the output generated by the active cochlea.

In human CHARGE patients, variable cochlear malformations have been reported including an overall reduction in cochlear height, modiolar defects that range from subtle dysplasias to severe partitioning defects (Mondini malformation), and dysplasia/hypoplasia of the basal and/or apical turns (Dhooge et al., 1998; Glueckert et al., 2010; Guyot et al., 1987; Haginomori et al., 2002; Morimoto et al., 2006; Wright et al., 1986). In some CHARGE individuals, the cochlear duct is shortened, yet there is a normal-appearing organ of Corti with a full complement of hair cells (Glueckert et al., 2010). In $Chd7^{Gt/+}$ mice, the cochlea is morphologically normal with the correct number of turns. There is also no evidence of cochlear HC loss in $Chd7^{Gt/+}$ mice, and individual HC morphology is normal with the exception of increased incidence of supernumerary rows of HCs, as in prior studies of *Chd7* mutant mice (Hawker et al., 2005; Kiernan et al., 2002; Lenz et al., 2010). It is possible that

the presence of a fourth row of OHCs causes a threshold elevation, a notion that is supported by the presence of these extranumerary hair cells predominantly in the low frequency area of the cochlea. Nevertheless, it is important to note many of the wild type mice also had some areas containing four rows of OHC and their hearing was normal.

Many mice were homozygous for the *Cdh23*^{ahl} locus, which predisposes to hearing loss that appears beginning at 8 weeks of age and typically affects responses to high frequency sounds (Noben-Trauth et al., 2003). We detected ABR shifts as early as 5 weeks of age that were more pronounced in the lower (4 and 16 kHz) frequencies; thus, it seems unlikely that homozygosity for *Cdh23*^{ahl} explains the HL phenotypes in *Chd7* mutant mice.

Neuronal defects in the cochlea of CHARGE patients may contribute to SNHL in these individuals since neuronal cell bodies are often displaced into the internal acoustic meatus (Glueckert et al., 2010). We observed no differences in peripheral cochlear fibers between *Chd7*$^{Gt/+}$ and wild type mice, suggesting that defects in the neural component of the inner ear may not explain the increased auditory thresholds in *Chd7*$^{Gt/+}$ mice. Despite normal cochlear and cochlear nerve anatomy, it is possible that other physiological impairments (undetected by the methods used here) may contribute to *Chd7*$^{Gt/+}$ HL. For example, *Chd7* mutant mice may have defects within the hair cell stereocilia, IHC/OHC synapses, IHC/OHC transduction channels or in neurotransmitter release/attenuation. Additional TEM and physiological analyses will be needed to identify the pathology which accounts for the SNHL.

4.4 Implications for *Chd7* expression during middle ear development

While vestibular function was not tested in this study, *Chd7* mutant mice exhibit circling behaviors, head bobbing, and semicircular canal dysgenesis (Bosman et al., 2005; Hurd et al., 2007). It is not known whether middle ear dysfunction also contributes to these vestibular phenotypes. Middle ear defects have been observed in other mouse mutants including *Otx2, Tbx1, Fgfr1, Pou3f4, Prx1/2, Hoxa1,* and *Hoxb1* (reviewed in (Fekete, 1999)). *Chd7* mutant mice have dosage dependent changes in expression of *Otx2* and *Tbx1* in the developing otocyst (Hurd et al., 2010). *Otx2* is expressed within the saccule and cochlea of the developing inner ear, and heterozygous *Otx2* mutant mice have malleal, incudal, and craniofacial abnormalities (Matsuo et al., 1995; Morsli et al., 1999). *Otx2* expression is also decreased in the developing olfactory placode and adult hypothalamus of *Chd7* mutant mice (Layman et al., 2011). One patient is reported to have anophthalmia, pituitary hypoplasia and ear abnormalities including HL in association with a 14q22-23 deletion that includes *OTX2* (Nolen et al., 2006). These observations suggest that *Chd7* may developmentally regulate *Otx2* in multiple tissues including the inner and middle ear, olfactory epithelium, brain and bone.

Tbx1, another gene implicated in both inner and middle ear development, is expressed within the pharyngeal arches, otic mesenchyme and otic epithelium, in a similar pattern to *Chd7* (Arnold et al., 2006; Hurd et al., 2010; Moraes et al., 2005). *Tbx1* is upregulated in *Chd7* mutant otocysts (Hurd et al., 2010). *Tbx1* gain-of-function mutant mice have SNHL, otitis media and defects in middle ear ossicles, particularly the stapes (Funke et al., 2001). There is also overlap in clinical phenotypes between CHARGE syndrome and Deletion 22q11 syndrome, including HL, craniofacial dysmorphisms and cardiac abnormalities. Haploinsufficiency for *TBX1* is thought to explain many of the developmental abnormalities in Deletion 22q11 syndrome (Reyes et al., 1999). Interestingly, *Tbx1;Chd7* double heterozygous mutant mice display a slightly more severe inner ear phenotype than *Chd7*$^{+/-}$ mice but there is no known direct interaction between *Chd7* and *Tbx1* (Randall et al., 2009). Instead, *Chd7* and *Tbx1* may share direct or indirect downstream gene targets during pharyngeal arch/middle ear development.

Fgfr1 mutant mice have abnormal stapes anatomy, increased compound action potentials and skeletal defects (Calvert et al., 2011). *Fgfr1* expression is decreased in *Chd7* mutant olfactory placodes (Layman et al., 2011), and may also have roles in inner and middle ear development. *Fgfr1;Chd7* double heterozygous mice die within the early postnatal period (Bergman et al., 2010). Inner ear defects of *Fgfr1-Chd7* heterozygotes are no more severe than single *Chd7* heterozygous mice (Bergman et al., 2010); however, no analysis of middle ear anatomy has been reported. Human mutations in *FGFR1* are responsible for Pfeiffer syndrome, whose clinical phenotypes include middle ear defects and conductive, sensorineural or mixed HL (Desai et al., 2010). The overlap in HL and middle ear phenotypes in mice/humans with *Chd7*, *Tbx1*, *Fgfr1* and *Otx2* mutations suggests common developmental genetic pathways in ear development.

Skeletal and limb defects have also been reported in several CHARGE patients (Gao et al., 2007; Wright et al., 2009). Some CHARGE individuals have an abnormally thickened bony prominence over the cochlear aperture covering the cochlear nerve, giving the cochlea an isolated or “trapped” appearance (Morimoto et al., 2006). Abnormal ankylosis observed within the stapes of *Chd7* mutant mice and trapped cochleae in CHARGE patients may also indicate common developmental mechanisms, such as incomplete mesenchymal transitions or altered cell fate switch before ossification. Interestingly, CHD7 deficiency in bone marrow mesenchymal cells changes their fate from osteoblasts to adipocytes (Takada et al., 2007). During middle ear development, the stapes is the last ossicle to form and to ossify, and the most severely affected middle ear ossicle in *Chd7* mutant mice. Similarly, within the inner ear, the lateral semicircular canal is the last canal to form and is uniformly affected in $Chd7^{Gt/+}$ mice (Adams et al., 2007; Hurd et al., 2007). Abnormal dose or timing of *Chd7* regulation/action within the ear may result in widespread tissue specific defects of mesenchymal transitions, ossification, and/or morphogenetic signaling cascades.

4.5 Implications for future therapy

The developmental importance of proper *Chd7* dosage (wild type, heterozygous mutant or homozygous mutant), combined with mature *Chd7* expression in the middle and inner ear, suggests pre- and/or post-natal opportunities for therapeutic intervention in CHARGE individuals. Successful replacement of *CHD7* or modification of its target genes may ultimately prove helpful *in utero* or even later in life. The expression of *CHD7* in mature ear tissues provides an opportunity for phenotypic rescue during post-developmental periods in the ear, and possibly other tissues that require this molecule for development and function. The survival of inner ear cells in mice with reduced *Chd7* dosage contributes to the feasibility of treatment for increasing the dose of the wild type gene product. In addition, protection from noise could provide Audiologists with guidelines for safe delivery of auditory signals via amplification by hearing aids or bone-anchored devices, especially after the air/bone gap is established in free field audiograms and DPOAEs are confirmed to be low or absent.

Acknowledgments

This work was supported by the Williams Professorship, the A. Alfred Taubman Medical Research Institute and the Berte and Alan Hirschfield Foundation (Y.R), NOHR (D.M.M), and NIH/NIDCD grants P30 DC05188 (Y.R and D.F.D) and DC009410 (D.M.M and Y.R).

Abbreviations

ABR	Auditory brainstem response
BAHA	Bone-anchored hearing aid

CHD7	Chromodomain helicase DNA-binding protein 7
dB SPL	Decibel Sound pressure level
DPOAE	Distortion Product Otoacoustic Emission
HL	Hearing loss
IHC	Inner hair cell
OHC	Outer hair cell
SEM	Scanning electron microscopy
SNHL	Sensorineural hearing loss

References

Abadie V, Wiener-Vacher S, Morisseau-Durand MP, Poree C, Amiel J, Amanou L, Peigne C, Lyonnet S, Manac'h Y. Vestibular anomalies in CHARGE syndrome: investigations on and consequences for postural development. Eur J Pediatr. 2000; 159:569–74. [PubMed: 10968232]

Adams ME, Hurd EA, Beyer LA, Swiderski DL, Raphael Y, Martin DM. Defects in vestibular sensory epithelia and innervation in mice with loss of Chd7 function: implications for human CHARGE syndrome. J Comp Neurol. 2007; 504:519–32. [PubMed: 17701983]

Admiraal RJ, Huygen PL. Vestibular areflexia as a cause of delayed motor skill development in children with the CHARGE association. Int J Pediatr Otorhinolaryngol. 1997; 39:205–22. [PubMed: 9152748]

Amiel J, Attiee-Bitach T, Marianowski R, Cormier-Daire V, Abadie V, Bonnet D, Gonzales M, Chemouny S, Brunelle F, Munnich A, Manach Y, Lyonnet S. Temporal bone anomaly proposed as a major criteria for diagnosis of CHARGE syndrome. Am J Med Genet A. 2001; 99:124–7.

Arnold JS, Braunstein EM, Ohyama T, Groves AK, Adams JC, Brown MC, Morrow BE. Tissue-specific roles of Tbx1 in the development of the outer, middle and inner ear, defective in 22q11DS patients. Hum Mol Genet. 2006; 15:1629–39. [PubMed: 16600992]

Bergman JE, Bosman EA, van Ravenswaaij-Arts CM, Steel KP. Study of smell and reproductive organs in a mouse model for CHARGE syndrome. Eur J Hum Genet. 2010; 18:171–7. [PubMed: 19809474]

Beyer LA, Odeh H, Probst FJ, Lambert EH, Dolan DF, Camper SA, Kohrman DC, Raphael Y. Hair cells in the inner ear of the pirouette and shaker 2 mutant mice. J Neurocytol. 2000; 29:227–40. [PubMed: 11276175]

Bosman EA, Penn AC, Ambrose JC, Kettleborough R, Stemple DL, Steel KP. Multiple mutations in mouse Chd7 provide models for CHARGE syndrome. Hum Mol Genet. 2005; 14:3463–76. [PubMed: 16207732]

Calvert JA, Dedos SG, Hawker K, Fleming M, Lewis MA, Steel KP. A missense mutation in Fgfr1 causes ear and skull defects in hush puppy mice. Mamm Genome. 2011; 22:290–305. [PubMed: 21479780]

Dallos P. Cochlear amplification, outer hair cells and prestin. Curr Opin Neurobiol. 2008; 18:370–6. [PubMed: 18809494]

Desai U, Rosen H, Mulliken JB, Gopen Q, Meara JG, Rogers GF. Audiologic findings in Pfeiffer syndrome. J Craniofac Surg. 2010; 21:1411–8. [PubMed: 20856029]

Dhooge I, Lemmerling M, Lagache M, Standaert L, Govaert P, Mortier G. Otological manifestations of CHARGE association. Ann Otol Rhinol Laryngol. 1998; 107:935–41. [PubMed: 9823842]

Edwards BM, Van Riper LA, Kileny PR. Clinical manifestations of CHARGE Association. Int J Pediatr Otorhinolaryngol. 1995; 33:23–42. [PubMed: 7558639]

Edwards BM, Kileny PR, Van Riper LA. CHARGE syndrome: a window of opportunity for audiologic intervention. Pediatrics. 2002; 110:119–26. [PubMed: 12093956]

Fekete DM. Development of the vertebrate ear: insights from knockouts and mutants. Trends Neurosci. 1999; 22:263–9. [PubMed: 10354604]

Funke B, Epstein JA, Kochilas LK, Lu MM, Pandita RK, Liao J, Bauerndistel R, Schuler T, Schorle H, Brown MC, Adams J, Morrow BE. Mice overexpressing genes from the 22q11 region deleted in velo-cardio-facial syndrome/DiGeorge syndrome have middle and inner ear defects. Human molecular genetics. 2001; 10:2549–56. [PubMed: 11709542]

Gao X, Gordon D, Zhang D, Browne R, Helms C, Gillum J, Weber S, Devroy S, Swaney S, Dobbs M, Morcuende J, Sheffield V, Lovett M, Bowcock A, Herring J, Wise C. CHD7 gene polymorphisms are associated with susceptibility to idiopathic scoliosis. American journal of human genetics. 2007; 80:957–65. [PubMed: 17436250]

Gehr DD, Janssen T, Michaelis CE, Deingruber K, Lamm K. Middle ear and cochlear disorders result in different DPOAE growth behaviour: implications for the differentiation of sound conductive and cochlear hearing loss. Hear Res. 2004; 193:9–19. [PubMed: 15219315]

Glueckert R, Rask-Andersen H, Sergi C, Schmutzhard J, Mueller B, Beckmann F, Rittinger O, Hoefsloot LH, Schrott-Fischer A, Janecke AR. Histology and synchrotron radiation-based microtomography of the inner ear in a molecularly confirmed case of CHARGE syndrome. Am J Med Genet A. 2010; 152A:665–73. [PubMed: 20186814]

Guyot JP, Gacek RR, DiRaddo P. The temporal bone anomaly in CHARGE association. Archives of Otolaryngology -- Head & Neck Surgery. 1987; 113:321–4. [PubMed: 3814379]

Haginomori S, Sando I, Miura M, Casselbrant ML. Temporal bone histopathology in CHARGE association. Ann Otol Rhinol Laryngol. 2002; 111:397–401. [PubMed: 12018323]

Harding GW, Bohne BA, Vos JD. The effect of an age-related hearing loss gene (Ahl) on noise-induced hearing loss and cochlear damage from low-frequency noise. Hear Res. 2005; 204:90–100. [PubMed: 15925194]

Hawker K, Fuchs H, Angelis MH, Steel KP. Two new mouse mutants with vestibular defects that map to the highly mutable locus on chromosome 4. Int J Audiol. 2005; 44:171–7. [PubMed: 15916118]

Hurd EA, Poucher HK, Cheng K, Raphael Y, Martin DM. The ATP-dependent chromatin remodeling enzyme CHD7 regulates pro-neural gene expression and neurogenesis in the inner ear. Development. 2010; 137:3139–50. [PubMed: 20736290]

Hurd EA, Capers PL, Blauwkamp MN, Adams ME, Raphael Y, Poucher HK, Martin DM. Loss of Chd7 function in gene-trapped reporter mice is embryonic lethal and associated with severe defects in multiple developing tissues. Mamm Genome. 2007; 18:94–104. [PubMed: 17334657]

Jongmans MC, Admiraal RJ, van der Donk KP, Vissers LE, Baas AF, Kapusta L, van Hagen JM, Donnai D, de Ravel TJ, Veltman JA, van Kessel A. Geurts, De Vries BB, Brunner HG, Hoefsloot LH, van Ravenswaaij CM. CHARGE syndrome: the phenotypic spectrum of mutations in the CHD7 gene. J Med Genet. 2006; 43:306–14. [PubMed: 16155193]

Karolyi IJ, Dootz GA, Halsey K, Beyer L, Probst FJ, Johnson KR, Parlow AF, Raphael Y, Dolan DF, Camper SA. Dietary thyroid hormone replacement ameliorates hearing deficits in hypothyroid mice. Mamm Genome. 2007; 18:596–608. [PubMed: 17899304]

Kiernan AE, Erven A, Voegeling S, Peters J, Nolan P, Hunter J, Bacon Y, Steel KP, Brown SD, Guenet JL. ENU mutagenesis reveals a highly mutable locus on mouse Chromosome 4 that affects ear morphogenesis. Mamm Genome. 2002; 13:142–8. [PubMed: 11919684]

Lalani SR, Safiullah AM, Fernbach SD, Harutyunyan KG, Thaller C, Peterson LE, McPherson JD, Gibbs RA, White LD, Hefner M, Davenport SL, Graham JM, Bacino CA, Glass NL, Towbin JA, Craigen WJ, Neish SR, Lin AE, Belmont JW. Spectrum of CHD7 Mutations in 110 Individuals with CHARGE Syndrome and Genotype-Phenotype Correlation. Am J Hum Genet. 2006; 78:303–14. [PubMed: 16400610]

Lanson BG, Green JE, Roland JT Jr. Lalwani AK, Waltzman SB. Cochlear implantation in Children with CHARGE syndrome: therapeutic decisions and outcomes. The Laryngoscope. 2007; 117:1260–6. [PubMed: 17507827]

Layman WS, Hurd EA, Martin DM. Reproductive dysfunction and decreased GnRH neurogenesis in a mouse model of CHARGE syndrome. Hum Mol Genet. 2011; 20:3138–3150. [PubMed: 21596839]

Layman WS, McEwen DP, Beyer LA, Lalani SR, Fernbach SD, Oh E, Swaroop A, Hegg CC, Raphael Y, Martens JR, Martin DM. Defects in neural stem cell proliferation and olfaction in Chd7 deficient mice indicate a mechanism for hyposmia in human CHARGE syndrome. Hum Mol Genet. 2009; 18:1909–23. [PubMed: 19279158]

Lemmerling M, Dhooge I, Mollet P, Mortier G, Van Cauwenberge P, Kunnen M. CT of the temporal bone in the CHARGE association. Neuroradiology. 1998; 40:462–5. [PubMed: 9730349]

Lenz DR, Dror AA, Wekselman G, Fuchs H, de Angelis M. Hrabe, Avrahamn KB. The inner ear phenotype pf Volchok (Vlk): An ENU-induced mouse model for CHARGE syndrome. Audiol Med. 2010:1–10.

Martin DM. Chromatin remodeling in development and disease: focus on CHD7. PLoS Genet. 2010; 6:e1001010. [PubMed: 20657659]

Matsuo I, Kuratani S, Kimura C, Takeda N, Aizawa S. Mouse Otx2 functions in the formation and patterning of rostral head. Genes & development. 1995; 9:2646–58. [PubMed: 7590242]

Moraes F, Novoa A, Jerome-Majewska LA, Papaioannou VE, Mallo M. Tbx1 is required for proper neural crest migration and to stabilize spatial patterns during middle and inner ear development. Mechanisms of development. 2005; 122:199–212. [PubMed: 15652707]

Morgan D, Bailey M, Phelps P, Bellman S, Grace A, Wyse R. Ear-nose-throat abnormalities in the CHARGE association. Arch Otolaryngol Head Neck Surg. 1993; 119:49–54. [PubMed: 8417743]

Morimoto AK, Wiggins RH 3rd, Hudgins PA, Hedlund GL, Hamilton B, Mukherji SK, Telian SA, Harnsberger HR. Absent semicircular canals in CHARGE syndrome: radiologic spectrum of findings. AJNR Am J Neuroradiol. 2006; 27:1663–71. [PubMed: 16971610]

Morsli H, Tuorto F, Choo D, Postiglione MP, Simeone A, Wu DK. Otx1 and Otx2 activities are required for the normal development of the mouse inner ear. Development. 1999; 126:2335–43. [PubMed: 10225993]

Noben-Trauth K, Zheng QY, Johnson KR. Association of cadherin 23 with polygenic inheritance and genetic modification of sensorineural hearing loss. Nat Genet. 2003; 35:21–3. [PubMed: 12910270]

Nolen LD, Amor D, Haywood A, St Heaps L, Willcock C, Mihelec M, Tam P, Billson F, Grigg J, Peters G, Jamieson RV. Deletion at 14q22-23 indicates a contiguous gene syndrome comprising anophthalmia, pituitary hypoplasia, and ear anomalies. American journal of medical genetics. 2006; 140:1711–8. [PubMed: 16835935]

Osborne MP, Comis SD. Preparation of inner ear sensory hair bundles for high resolution scanning electron microscopy. Scanning Microsc. 1991; 5:555–64. [PubMed: 1947938]

Park K, Ueno K, Lim DJ. Developmental anatomy of the eustachian tube and middle ear in mice. Am J Otolarygol. 1992; 13:93–100.

Pau H, Hawker K, Fuchs H, De Angelis MH, Steel KP. Characterization of a new mouse mutant, flouncer, with a balance defect and inner ear malformation. Otol Neurotol. 2004; 25:707–13. [PubMed: 15353999]

Qin Z, Wood M, Rosowski JJ. Measurement of conductive hearing loss in mice. Hear Res. 2010; 263:93–103. [PubMed: 19835942]

Randall V, McCue K, Roberts C, Kyriakopoulou V, Beddow S, Barrett AN, Vitelli F, Prescott K, Shaw-Smith C, Devriendt K, Bosman E, Steffes G, Steel KP, Simrick S, Basson MA, Illingworth E, Scambler PJ. Great vessel development requires biallelic expression of Chd7 and Tbx1 in pharyngeal ectoderm in mice. J Clin Invest. 2009; 119:3301–3310. [PubMed: 19855134]

Reyes MR, LeBlanc EM, Bassila MK. Hearing loss and otitis media in velo-cardio-facial syndrome. International journal of pediatric otorhinolaryngology. 1999; 47:227–33. [PubMed: 10321777]

Sanlaville D, Etchevers HC, Gonzales M, Martinovic J, Clement-Ziza M, Delezoide AL, Aubry MC, Pelet A, Chemouny S, Cruaud C, Audollent S, Esculpavit C, Goudefroye G, Ozilou C, Fredouille C, Joye N, Morichon-Delvallez N, Dumez Y, Weissenbach J, Munnich A, Amiel J, Encha-Razavi F, Lyonnet S, Vekemans M, Attie-Bitach T. Phenotypic spectrum of CHARGE syndrome in fetuses with CHD7 truncating mutations correlates with expression during human development. J Med Genet. 2006; 43:211–217. [PubMed: 16169932]

Shah UK, Ohlms LA, Neault MW, Willson KD, McGuirt WF Jr. Hobbs N, Jones DT, McGill TJ, Healy GB. Otologic management in children with the CHARGE association. Int J Pediatr Otorhinolaryngol. 1998; 44:139–47. [PubMed: 9725530]

Takada I, Mihara M, Suzawa M, Ohtake F, Kobayashi S, Igarashi M, Youn MY, Takeyama K, Nakamura T, Mezaki Y, Takezawa S, Yogiashi Y, Kitagawa H, Yamada G, Takada S, Minami Y, Shibuya H, Matsumoto K, Kato S. A histone lysine methyltransferase activated by non-canonical Wnt signalling suppresses PPAR-gamma transactivation. Nat Cell Biol. 2007; 9:1273–85. [PubMed: 17952062]

Tellier AL, Cormier-Daire V, Abadie V, Amiel J, Sigaudy S, Bonnet D, de Lonlay-Debeney P, Morrisseau-Durand MP, Hubert P, Michel JL, Jan D, Dollfus H, Baumann C, Labrune P, Lacombe D, Philip N, LeMerrer M, Briard ML, Munnich A, Lyonnet S. CHARGE syndrome: report of 47 cases and review. American Journal of Medical Genetics. 1998; 76:402–9. [PubMed: 9556299]

Thelin JW, Mitchell JA, Hefner MA, Davenport SL. CHARGE syndrome. Part II. Hearing loss. Int J Pediatr Otorhinolaryngol. 1986; 12:145–63. [PubMed: 3570681]

Vissers LE, van Ravenswaaij CM, Admiraal R, Hurst JA, de Vries BB, Janssen IM, van der Vliet WA, Huys EH, de Jong PJ, Hamel BC, Schoenmakers EF, Brunner HG, Veltman JA, van Kessel AG. Mutations in a new member of the chromodomain gene family cause CHARGE syndrome. Nat Genet. 2004; 36:955–7. [PubMed: 15300250]

Wiener-Vacher SR, Amanou L, Denise P, Narcy P, Manach Y. Vestibular function in children with the CHARGE association. Arch Otolaryngol Head Neck Surg. 1999; 125:342–7. [PubMed: 10190809]

Wright CG, Brown OE, Meyerhoff WL, Rutledge JC. Auditory and temporal bone abnormalities in CHARGE association. Annals of Otology, Rhinology & Laryngology. 1986; 95:480–6.

Wright EM, O'Connor R, Kerr BA. Radial aplasia in CHARGE syndrome: a new association. European journal of medical genetics. 2009; 52:239–41. [PubMed: 19375527]

Zentner GE, Layman WS, Martin DM, Scacheri PC. Molecular and phenotypic aspects of CHD7 mutation in CHARGE syndrome. American journal of medical genetics. Part A. 2010; 152A:674–86. [PubMed: 20186815]

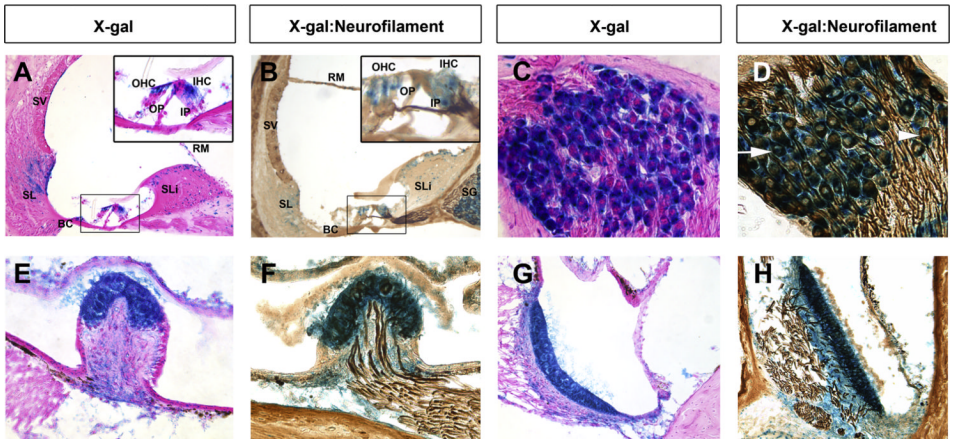

Figure 1. *Chd7* is expressed in neurons of the mature cochlea and vestibular sensory epithelia

Coronal cryosections of adult $Chd7^{Gt/+}$ cochleae (A-D), lateral canal crista ampullaris (E,F) or utricle (G,H) stained for β-galactosidase activity with X-gal and co-stained with either eosin (A,C,E,G) or anti-neurofilament immunohistochemistry (B,D,F,H). (A-D) β-galactosidase activity is present in the stria vascularis (SV), Reissner's membrane (RM), spiral limbus (SLi), spiral ligament (SL), Boettcher's cells (BC), and spiral ganglion (SG). Enlarged insets in A and B show β-galactosidase activity in outer hair cells (OHC), inner hair cells (IHC), inner pillar cells (IP) and outer pillar cells (OP) of the organ of Corti. (D) β-galactosidase activity was observed within the cytoplasm of most spiral ganglion neurons (arrow). β-galactosidase negative, neurofilament positive cells (arrowhead) are also observed. (E-H) Dense β-galactosidase activity was present throughout the vestibular sensory epithelia and co-labels with anti-neurofilament (F,H) demonstrating *Chd7* expression within vestibular neurons.

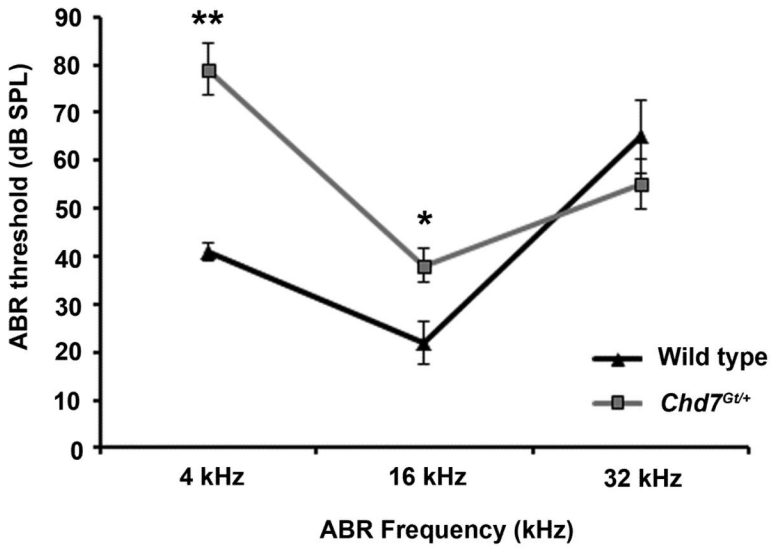

Figure 2. *Chd7*$^{Gt/+}$ mice display hearing loss

ABR tests showed elevated thresholds at 4 and 16 kHz in *Chd7*$^{Gt/+}$ mice compared to wild type sex- and age-matched littermates. *, $p < 0.009$; **, $p < 0.0001$.

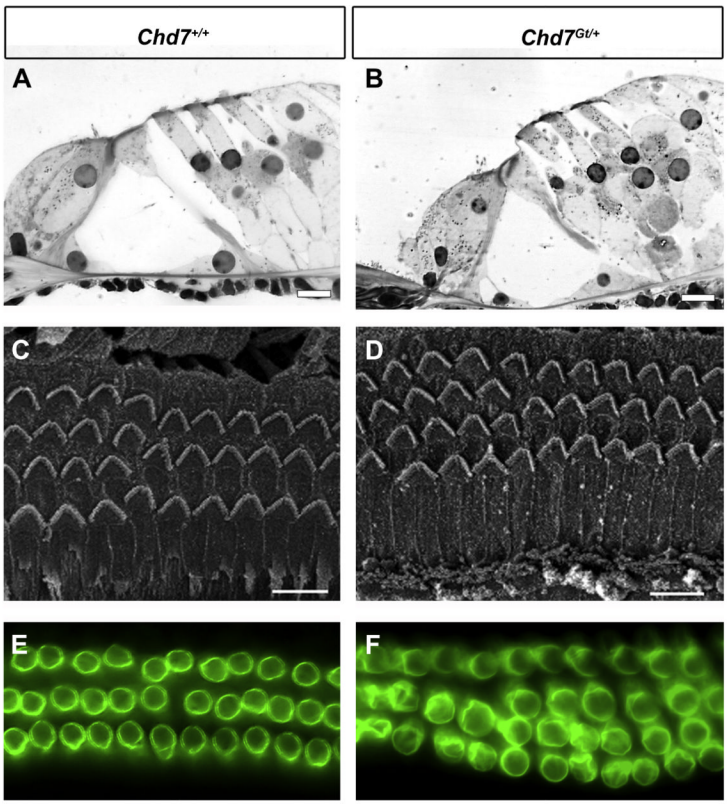

Figure 3. Cochlear anatomy and outer hair cell integrity is normal in *Chd7*$^{Gt/+}$ mice

Light microscopy (A-B), scanning electron microscopy (C-D) and Prestin epifluorescence (E-F) of the organ of Corti of wild type (A, C, E) and *Chd7*$^{Gt/+}$ mice (B, D, F) at 6 weeks of age. (A-B) Histology for hair cells and non-sensory cells in the organ of Corti was similar in *Chd7*$^{Gt/+}$ and wild type mice. (C-D) OHCs appear normal and the organization of surface morphology is similar between *Chd7*$^{Gt/+}$ and wild type ears. In both wild type and *Chd7*$^{Gt/+}$ mice, occasional stretches of 4 rows of OHCs are seen. (D-F) Prestin immunostaining of OHCs is unchanged in *Chd7*$^{Gt/+}$ cochleae (D) compared to wild type (C) mice. Fourth row OHCs display Prestin staining that appears identical to that seen in the other three rows. Scale bars are 10 μm in A and B, and 20 μm in C and D.

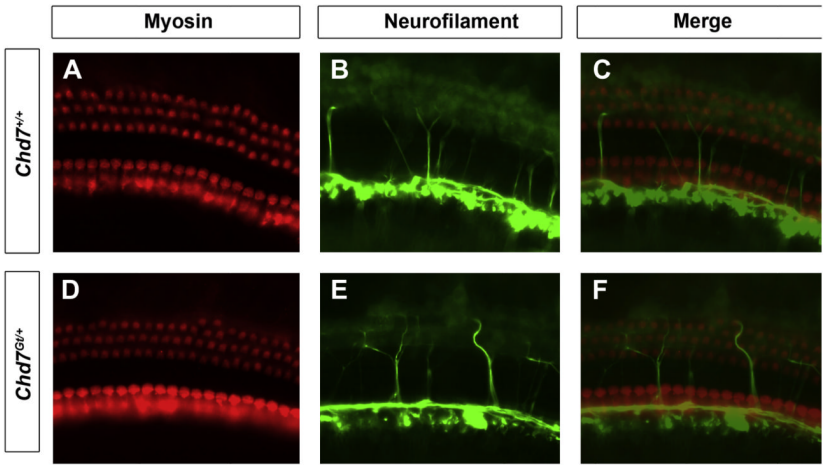

Figure 4. Hair cell innervation appears normal in *Chd7*$^{Gt/+}$ mice

Whole mount immunofluorescence of wild type (A-C) or *Chd7*$^{Gt/+}$ (D-F) mouse cochleae stained with anti-myosin VIIA (A,D) and anti-neurofilament (B,E). Merged images (C,F) show similar innervation of hair cells in the cochleae of wild type (C) and *Chd7*$^{Gt/+}$ mice (F).

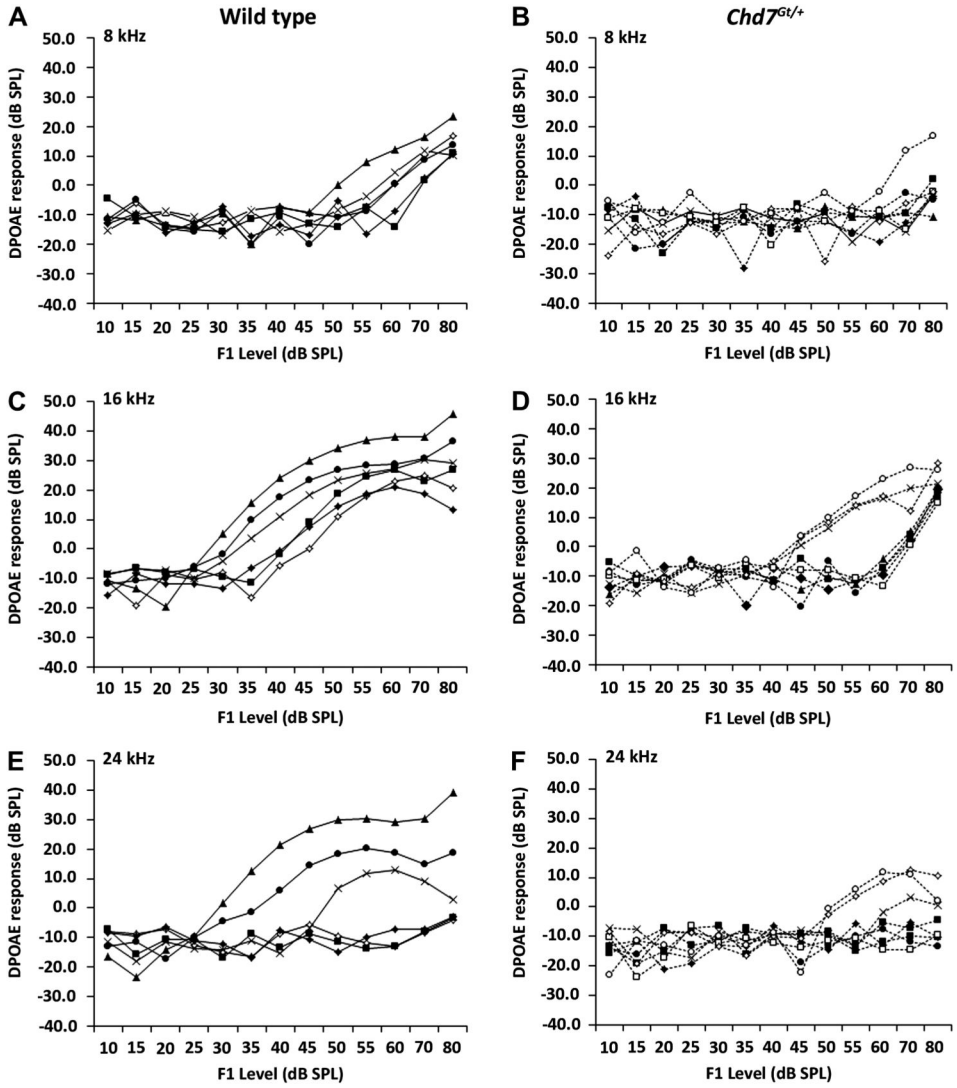

Figure 5. *Chd7*$^{Gt/+}$ mice have reduced cochlear emissions

DPOAEs were performed on adult wild type (A,C,E) and *Chd7*$^{Gt/+}$ mice (B,D,F), who also had ABRs performed (N=7 each) (Fig. 2). Flattened DPOAE were observed in the majority of *Chd7*$^{Gt/+}$ mice.

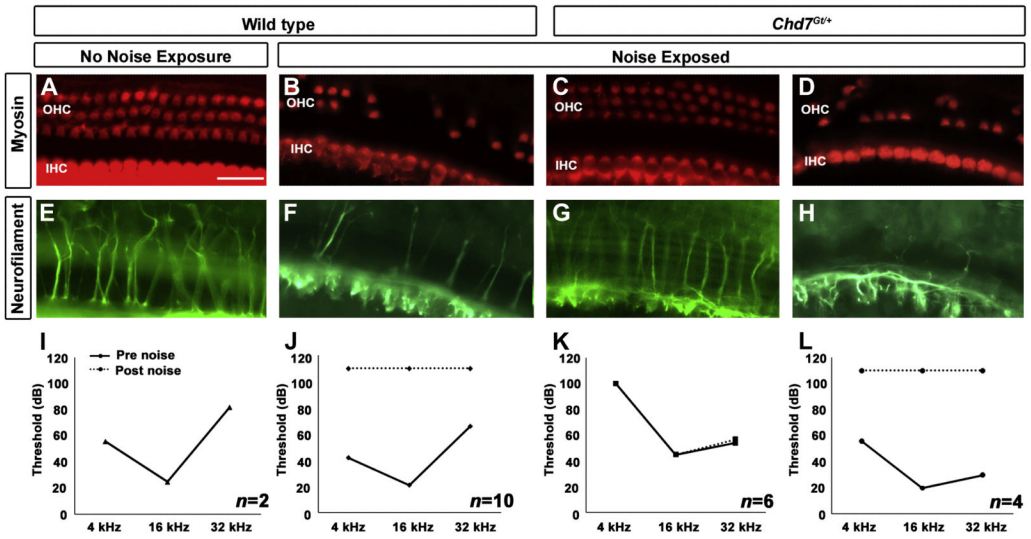

Figure 6. Resistance of *Chd7*$^{Gt/+}$ mice to noise exposure

Adult wild type (A,B,E,F) or *Chd7*$^{Gt/+}$ mice (C,D,G,H) were either exposed (B-D,F-H) or not exposed (A,E) to 123 dB SPL broadband noise for 4.5 hrs. ABRs were tested pre- and post-noise exposure (I-L) and dissected cochleae were stained with anti-myosin (A-D) and anti-neurofilament (E-H). (A,E,I) Unexposed wild type mice (N=2) had no loss of hair cells, normal innervation, and unchanged ABRs. Wild type noise-exposed mice (N=10) had severe loss of OHCs, mild loss of IHCs (B), decreased innervation (F), and elevated ABR thresholds (J). The majority of noise-exposed *Chd7*$^{Gt/+}$ mice (N=6/10) displayed no IHC or OHC loss (C), normal innervation (G), and unchanged ABR thresholds (K). Some *Chd7*$^{Gt/+}$ mice (N=4/10) exhibited damage/loss of IHCs and OHCs (D), reduced innervation (H), and elevated ABR thresholds (L) after noise exposure.

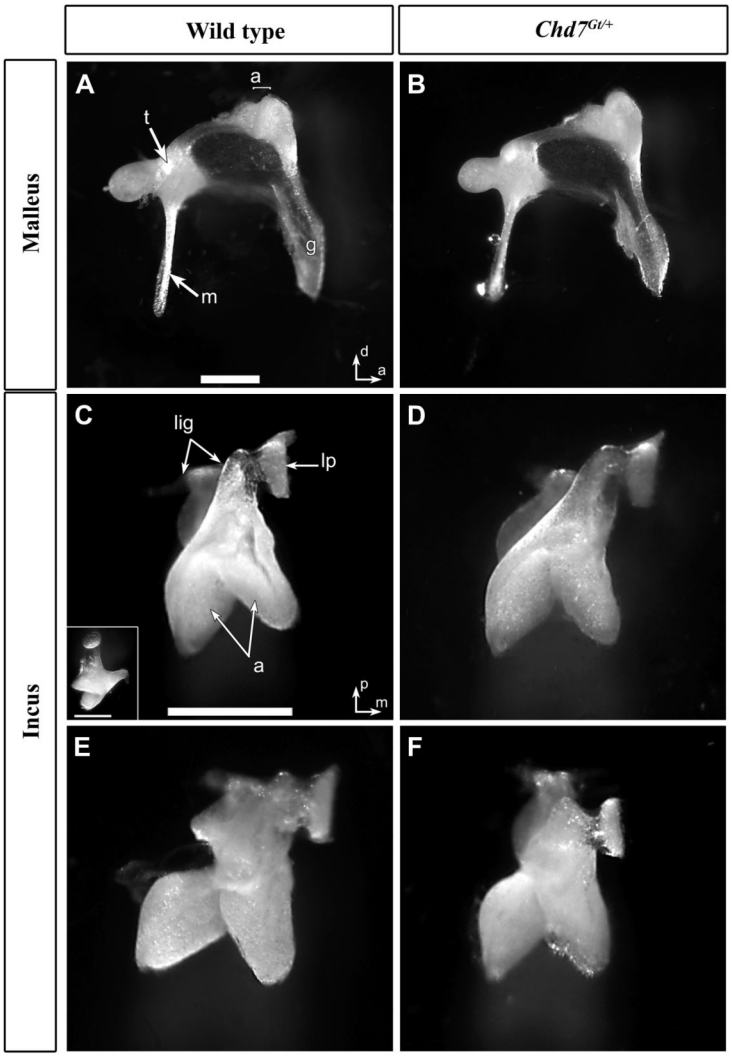

Figure 7. Malleus and incus are normal in *Chd7*$^{Gt/+}$ mice

Medial views of mallei (A,B) and ventral view of incudes (C-F) from wild type (A,C,E) and *Chd7*$^{Gt/+}$ (B,D,E) mice. Mallei from *Chd7*$^{Gt/+}$ mice (B) were similar to those of wild type (A). Normal incus morphology (C, D) and variant forms (E,F) with the lateral component of the articulation structure abnormally shaped and incompletely attached to the main body. Scale bars =0.5 mm. Inset in C shows medial view. Other abbreviations: (m) manubrium of malleus, (a) articulation surfaces of malleus and incus joint, (t) tubercle, (g) gonial angle, (lig) attachment points of suspensory ligaments of incus, (lp) lenticular process.

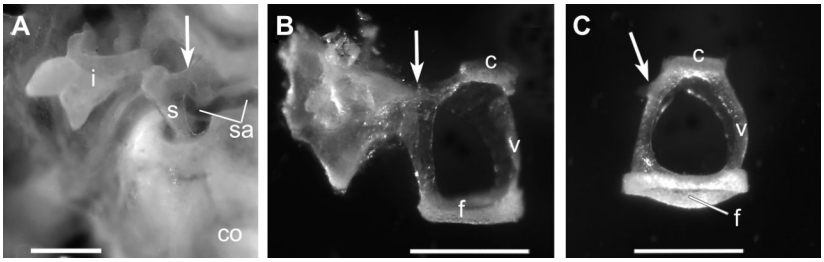

Figure 8. Stapedial defects are present in the majority of *Chd7*$^{Gt/+}$ mice

(A) Ventro-lateral i*n situ* view of the stapes (s) and incus (i) from a *Chd7*$^{Gt/+}$ mouse demonstrating ankylosis of dorsal crus of stapes to the dorsal wall of the middle ear space (arrow). (B) Excised stapes and part of the dorsal wall, in anterior view from a *Chd7*$^{Gt/+}$ mouse, showed a thick connection between the dorsal crus and the wall (arrow) and flattened footplate (f). (C) Normal stapedial anatomy of a wild type stapes with bowed footplate and arched ventral crus (v). The arrow in each panel indicates the insertion site of the stapes muscle tendon. Other abbreviations: (co) cochlea, (sa) stapedial artery, (c) capitulum of stapes. Scale bars = 0.5 mm.

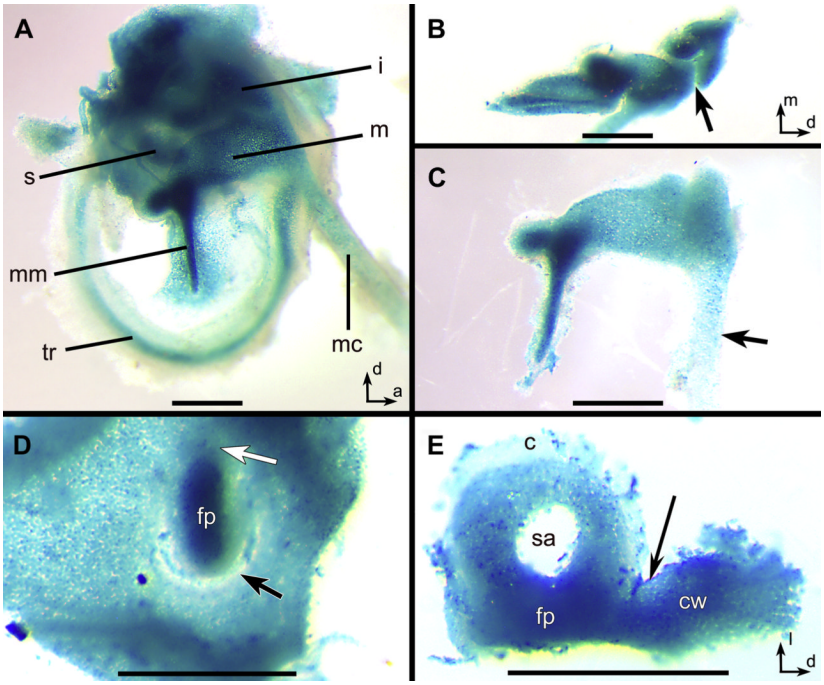

Figure 9. *Chd7* is expressed in the early postnatal middle ear ossicles

(A-C) β-galactosidase activity was observed in the malleus (m), incus (i) and stapes (s), in the tympanic ring (tr), Meckel's cartilage (mc), and in the tympanic membrane adjacent to manubrium of the malleus (mm) from a postnatal day 1 $Chd7^{Gt/+}$ mouse. (B) X-gal staining was observed throughout the incus except at the location of the joint between malleus and incus (arrow). (C) Intense β-galactosidase activity was observed within the posterior malleus with a decreasing gradient along Meckel's cartilage (arrow). (D) Incomplete separation of the stapedial footplate (fp) from the cochlear wall (black arrow) and continuity of label between footplate and wall was especially dense at the anterior end (white arrow). (E) Excised stapes and cochlear wall fragment (cw) showing continuity between wall and footplate (arrow). Other Abbreviations: (c) capitulum, (sa) foramen for the stapedial artery. Scale bars= 0.5 mm.